Published in final edited form as:

J Hepatol. 2017 May ; 66(5): 1037–1046. doi:10.1016/j.jhep.2017.01.022.

NLRP3 inflammasome blockade reduces liver inflammation and fibrosis in experimental NASH in mice

Auvro R. Mridha[1,†], **Alexander Wree**[2,3,†], **Avril A.B. Robertson**[4], **Matthew M. Yeh**[5], **Casey D. Johnson**[3], **Derrick M. Van Rooyen**[1], **Fahrettin Haczeyni**[1], **Narci C.-H. Teoh**[1], **Christopher Savard**[6], **George N. Ioannou**[6], **Seth L. Masters**[7], **Kate Schroder**[4], **Matthew A. Cooper**[4], **Ariel E. Feldstein**[3], and **Geoffrey C. Farrell**[1,*]

[1]Liver Research Group, ANU Medical School, Australian National University at The Canberra Hospital, Garran, ACT, Australia;

[2]Department of Internal Medicine III, RWTH-Aachen University Hospital, Aachen, Germany;

[3]Department of Pediatrics, University of California – San Diego, La Jolla, San Diego, CA, United States;

[4]Institute for Molecular Bioscience, University of Queensland, St Lucia, QLD, Australia;

[5]Department of Pathology, University of Washington, Seattle, WA, United States;

[6]Department of Gastroenterology and Hepatology, Veterans Affairs Puget Sound Health Care System and University of Washington, Seattle, WA, United States;

[7]The Walter and Eliza Hall Institute, Parkville, VIC, Australia

[*]Corresponding author. Address: Gastroenterology and Hepatology Unit, The Canberra Hospital, PO Box 111, Woden, ACT 2605, Australia. Fax: +61 2 62443235. geoff.farrell@anu.edu.au (G.C. Farrell).

Authors' contributions

Auvro R Mridha: experimental design and acquisition of data; analysis and interpretation of data, statistical analysis, drafting of figures, intellectual input and critical review of manuscript. Alexander Wree: experimental design and acquisition of data; analysis and interpretation of data, statistical analysis, drafting of figures and critical review of manuscript. Avril AB Robertson: experimental design and acquisition of data; interpretation of data and critical review of manuscript. Matthew M Yeh: acquisition of data; interpretation of data and critical review of manuscript. Casey D Johnson: technical support and acquisition of data, review of manuscript. Derrick M Van Rooyen: technical support and acquisition of data, review of manuscript. Fahrettin Haczeyni: technical support and acquisition of data, review of manuscript. Narci C-H Teoh: study design, data interpretation and critical review of manuscript. Christopher Savard: acquisition of data, critical review of manuscript. Fahrettin Haczeyni: technical support and acquisition of data, review of manuscript. Narci C-H Teoh: study design, data interpretation and critical review of manuscript. George N Ioannou: study design, data interpretation and critical review of manuscript. Seth L Masters: study conceptualization and important intellectual contribution, critical review of manuscript. Kate Schroder: important intellectual contribution, critical review of manuscript. Matthew A Cooper: study conceptualization, experimental design and important intellectual contribution, obtained funding, data interpretation and critical review of manuscript. Ariel E Feldstein: study conceptualization, experimental design and important intellectual contribution, obtained funding, data interpretation and critical review of manuscript. Geoffrey C Farrell: study conceptualization, experimental design and important intellectual contribution, obtained funding, data interpretation, drafted and finalized the manuscript.

[†]These authors contributed equally as joint first authors.

Conflict of interest

ARM, AW, MMY, CDJ, DVR, FH, NCT, CS, GNI, SLM, AEF and GCF have nothing to disclose. AABR, KS, and MAC are co-inventors on a patent application filed by The University of Queensland describing novel small molecules inhibitors of the NLRP3 inflammasome. However, none of these new molecules are described in the present work, which is limited to the public domain, non-patented compound MCC950. Hence there is no direct conflict of interest in this work describing the role of MCC950 in NASH, but the commercial association with other inhibitors of the inflammasome described in said patent application are declared.

Supplementary data

Supplementary data associated with this article can be found, in the online version, at http://dx.doi.org/10.1016/j.jhep.2017.01.022.

Abstract

Background & Aims: NOD-like receptor protein 3 (NLRP3) inflammasome activation occurs in Non-alcoholic fatty liver disease (NAFLD). We used the first small molecule NLRP3 inhibitor, MCC950, to test whether inflammasome blockade alters inflammatory recruitment and liver fibrosis in two murine models of steatohepatitis.

Methods: We fed *foz/foz* and wild-type mice an atherogenic diet for 16 weeks, gavaged MCC950 or vehicle until 24 weeks, then determined NAFLD phenotype. In mice fed an methionine/choline deficient (MCD) diet, we gavaged MCC950 or vehicle for 6 weeks and determined the effects on liver fibrosis.

Results: In vehicle-treated *foz/foz* mice, hepatic expression of NLRP3, pro-IL-1β, active caspase-1 and IL-1β increased at 24 weeks, in association with cholesterol crystal formation and NASH pathology; plasma IL-1β, IL-6, MCP-1, ALT/AST all increased. MCC950 treatment normalized hepatic caspase 1 and IL-1β expression, plasma IL-1β, MCP-1 and IL-6, lowered ALT/AST, and reduced the severity of liver inflammation including designation as NASH pathology, and liver fibrosis. *In vitro*, cholesterol crystals activated Kupffer cells and macrophages to release IL-1β; MCC950 abolished this, and the associated neutrophil migration. MCD diet-fed mice developed fibrotic steatohepatitis; MCC950 suppressed the increase in hepatic caspase 1 and IL-1β, lowered numbers of macrophages and neutrophils in the liver, and improved liver fibrosis.

Conclusion: MCC950, an NLRP3 selective inhibitor, improved NAFLD pathology and fibrosis in obese diabetic mice. This is potentially attributable to the blockade of cholesterol crystal-mediated NLRP3 activation in myeloid cells. MCC950 reduced liver fibrosis in MCD-fed mice. Targeting NLRP3 is a logical direction in pharmacotherapy of NASH.

Lay summary: Fatty liver disease caused by being overweight with diabetes and a high risk of heart attack, termed non-alcoholic steatohepatitis (NASH), is the most common serious liver disease with no current treatment. There could be several causes of inflammation in NASH, but activation of a protein scaffold within cells termed the inflammasome (NLRP3) has been suggested to play a role. Here we show that cholesterol crystals could be one pathway to activate the inflammasome in NASH. We used a drug called MCC950, which has already been shown to block NLRP3 activation, in an attempt to reduce liver injury in NASH. This drug partly reversed liver inflammation, particularly in obese diabetic mice that most closely resembles the human context of NASH. In addition, such dampening of liver inflammation in NASH achieved with MCC950 partly reversed liver scarring, the process that links NASH to the development of cirrhosis.

Keywords

NAFLD; NLRP3; Inflammasomes; Cholesterol crystals; Kupffer cells; Hepatocytes; Interleukin-1β; Fibrosis; Diet; atherogenic; Methionine; NLR proteins

Introduction

Non-alcoholic fatt y liver disease (NAFLD) increases standardised mortality from cardiovascular events, common cancers, cirrhosis and hepatocellular carcinoma [1,2]. Adverse liver outcomes are confined to the 10–25% of NAFLD patients with liver fibrosis,

particularly with the pathology of steatohepatitis (NASH) [3,4]. NASH occurs when overnutrition is complicated by insulin resistance and metabolic syndrome [2,5,6], particularly with a personal or family history of type 2 diabetes. Despite these connections, detailed mechanisms linking metabolic obesity to liver pathology are unclear. The most compelling concept is that hepatocyte injury results from lipotoxicity, a consequence of accumulated toxic lipid species [6,7]. Lipotoxicity, via release of danger-activated molecular patterns (DAMPs) from injured hepatocytes, and the gut microbiome via release of pathogen-activated molecular patterns (PAMPs) such as lipopolysaccharide (LPS) activate innate immunity to cause liver inflammation [8–10].

Innate immunity involves signalling via pattern recognition receptors, such as the Toll-like receptors (TLRs). During the last few years another trigger for liver inflammation in NAFLD has been identified as the NOD-like receptor protein 3 (NLRP3) inflammasome [11–22]. Inflammasomes are multiprotein scaffolds that respond to noxious signals (PAMPs, DAMPs) to recruit the adapter protein ASC and pro-caspase 1, thereby activating caspase 1 by autocatalysis [18,21,22]. Since the outcomes include programed cell death (pyroptosis), inflammation and fibrosis [16,19,22], the threshold for inflammasome activation requires a double activation signal. For the NLRP3 inflammasome, which is highly expressed in liver, the first signal is often LPS, but TNF-α and IL-1β are among other signal-1 molecules pertinent to NASH [16,19,22]. Factors that potentially provide the second signal include ATP, amyloid, uric acid and cholesterol crystals [23,24], while oxidative stress and potassium ion transport are related to the effector pathways of NLRP3 activation. In dietary and nutrient deficiency fatty liver diseases, increased hepatic expression of *Nlrp3, Asc* and *Casp1* accompanies liver inflammation [11,14,18,25]. NLRP3 activation occurs in human NASH [11,20], while experiments in *Nlrp3*$^{-/-}$, *Casp1*$^{-/-}$ and *Asc*$^{-/-}$ mice indicate NLRP3 activation is mechanistically important for NAFLD [11,13,20]. Until now, however, it has not been possible to test whether requirement for NLRP3 activation in the initiation and perpetuation of liver inflammation in NASH is obligatory, using intervention experiments. Further, we note that earlier studies did not use mice with metabolic syndrome, the invariable context of NASH in humans [1,2,5,6]. Development of MCC950 as a firstin-class, highly potent and selective small molecule inhibitor of NLRP3 [26], and characterization of a hyperphagic obesity mouse model of NASH linked to type 2 diabetes and metabolic syndrome [27–30], allowed us to conduct such studies, as reported here.

Cholesterol crystals activate NLRP3 in LPS-exposed macrophages [23,24]. Recently, cholesterol crystals have been observed in livers of human NASH and murine NASH models, including the one used for the present experiments [27,31]. Here, we first showed that cholesterol crystals activate NLRP3 in LPS-exposed Kupffer cells (KCs), bone marrow macrophages (BMMs), but minimally (if at all) in hepatocytes; 10 nM MCC950 inhibited such activation, as well as the resultant neutrophil migration in response to conditioned media from macrophages exposed to cholesterol crystals. We then conducted simultaneous studies in San Diego, CA and Canberra, Australia to test the efficacy of MCC950 for preventing or reversing liver injury, inflammation and fibrosis in two entirely different models of experimental steatohepatitis. Appetite-defective *foz/foz* mice are an overnutrition model in which NASH accompanies the onset of obesity and its metabolic complications, including diabetes and hypercholesterolemia [27–30]. The methionine and choline deficient

(MCD) dietary model causes severe steatohepatitis with liver fibrosis, whose pathogenesis involves hepatic oxidative stress as observed in human NASH [32,33]. Taken together, these novel findings provide robust support for the proposal that pharmacological blockade of NLRP3 activation in the liver can improve NASH pathology and modulate other forms of steatohepatitis, including its most critical outcome of liver fibrosis.

Materials and methods

Animal models

Animal experiments were approved by Animal Experimentation Ethics Committees of Australian National University (Canberra) and UC San Diego.

Atherogenic diet-fed foz/foz model

Groups (n = 11–13) of female *Alms1* mutant (*foz/foz*) mice or wild-type (Wt) litter-mates were fed atherogenic diet (23% fat, 45% carbohydrate, 20% protein, 0.2% cholesterol; SF03020, Specialty Feeds, Glenn Forrest, Western Australia) for 16 weeks, when *foz/foz* mice weighed >60 g and exhibited hyperinsulinemia, diabetes, hypertension, hypercholesterolemia, hypoadiponectinemia, and NASH with fibrosis [29,30]. From 16 weeks, mice were gavaged MCC950 (20 mg/kg body weight) or vehicle (0.9% NaCl) every day, 5 days/week until 24 weeks (Supplementary Fig. 1A). Venous blood samples (~0.2 ml) were obtained by cheek bleeding at 15 and 20 weeks. At 24 weeks, mice were fasted 4 h to determine blood glucose (Accu-Check glucometer, Roche Diagnostics), anesthetized (ketamine and xylazine), plasma and liver collected and processed for histological and molecular readouts [29,30].

Methionine and choline deficient diet model

Since 2000 [32], this mouse model has been used extensively to cause severe steatohepatitis and fibrosis, resembling human NASH pathology [28]. Groups (n = 8) of 8-week-old male C57BL/6 (B6) mice were placed on MCD diet (TD90262, Teklad Mills, Madison, WI), controls were fed the identical diet supplemented with methionine and choline (MCS) (TD94149, Teklad Mills). MCD-fed mice and MCS controls were divided into groups receiving MCC950 (10 mg/kg body weight in 0.9% NaCl every day for 5 days, followed by 20 mg/kg every second day up to 6 weeks), or vehicle by gavage. At the end of experiments, mice were anesthetized, liver and plasma collected [19,20]. In a second experiment, mice (n = 5–6/group) were fed MCD diet for 6 weeks, during the last 2 weeks they were gavaged every day with MCC950 (20 mg/kg) or vehicle before experiments were completed.

Cholesterol crystal preparation

Hydrated cholesterol crystals, prepared as described [24], were homogenized to obtain crystals <10 μm in diameter, and suspended in culture media before addition to cells.

Isolation and culture of bone marrow-derived macrophages, primary hepatocytes, Kupffer cells, and neutrophil chemotaxis studies

Using 8–10-week-old female B6 mice, bone marrow cells were extracted and differentiated (7 days) into BMMs in murine L929 media (diluted 1:10 in RPMI with 10% FBS). Morphology was checked by Wright-Giemsa staining, phenotype by Mac1 and F4/80 double-positive cells (flow cytometry). In selected experiments, we isolated/cultured BMMs from *Tlr4*$^{-/-}$ mice (gift of Shaun Summers, Monash Medical Centre, Clayton, VIC), and *Myd88*$^{-/-}$ mice (Australian Phenomics Facility, Canberra), all B6. Hepatocytes were isolated by collagenase perfusion [30,34], seeded onto plates coated with collagen (Gibco, Carlsbad, CA), and cultured in Williams' E with 1% bovine serum albumin (Sigma-Aldrich, St Louis, MO), 10 mM HEPES, 10 mM nicotinamide, 100 U/ml penicillin and 100 μg/ml streptomycin. KCs were isolated from non-parenchymal cells of collagenase-perfused mouse liver [35]. Following pre-incubation with LPS (50 pg/ml) for 1 h (followed by washing), cholesterol crystals were added at concentrations indicated in the figure legends. We measured NLRP3 activation and inhibition by 10 nM MCC950 as IL-1β release into culture medium (ELISA). Neutrophil chemotaxis was performed as described [36] using recombinant mouse(rm)-TNFα as positive chemoattractant.

Analysis of plasma proteins

Plasma insulin, adiponectin, monocyte chemoattractant protein (MCP)-1, IL-1β, IL-6 and IL-18 were measured by ELISAs (Insulin, Millipore, USA; others, R&D Systems, Minneapolis, MN).

Assessment of liver injury, liver pathology and fibrosis

Plasma alanine aminotransferase (ALT) and aspartate aminotransferase (AST) were assayed by auto-analyser (Clinical Chemistry, ACT Pathology). Liver samples were fixed in 10% neutral-buffered formalin and paraffin embedded. H&E-stained liver sections were assessed blind by an experienced liver pathologist (MMY) for steatosis, inflammation and ballooning, combined as NAFLD activity score (NAS), and designation as: "definite NASH", "borderline NASH", "NAFLD but not NASH", or "not NAFLD". To demonstrate fibrosis, liver sections were stained 2 h with picric acid containing 0.1% fast green and 0.1% Sirius Red. Fibrosis severity determined by collagen densitometry [30,37].

Hepatic proteins

Hepatic proteins were estimated by Western immunoblot, [19,20,29,30,37] (anti-body conditions provided on request). For tissue protein expression studies, immunohistochemistry was performed [12,19,20,30,31,37]. NF-κB p65 positive nuclei (in hepatocytes and inflammatory cells) and MPO positive neutrophils were counted and numbers expressed per 100 hepatocytes. F4/80-positive staining was used to identify activated macrophages and KCs surrounding steatotic hepatocytes to form crown-like structures (CLS). For each liver section, 10 random fields (400× magnification) were counted and mean value used.

Hepatic mRNA expression

We determined hepatic expression of specific mRNAs by reverse-transcriptase quantitative PCR (RT-qPCR), following extraction of total RNA from liver tissue [19,20]. Primer sequences in Supplementary Table 1. Expression of mRNA was relative β2-microglobulin (B2M).

Statistical analyses

For experiments involving 2 groups where distribution of data was not clearly parametric, Mann-Whitney *U* tests were performed with GraphPad Prism Software Inc, CA, Version 5.03. For experiments involving 3 or more groups, data were evaluated using one-way ANOVA with multiple comparison *post hoc* analysis. Data are expressed as mean ± SEM, or as absolute number or percentage for categorical variables. The number of animals or measurements in each group is indicated in the figure legends. The significance level was set at $\alpha = 5\%$ for all comparisons.

Results

Cholesterol crystals activate NLRP3 in wild-type but not Myd88$^{-/-}$ macrophages, Kupffer cells and hepatocytes

The high free cholesterol content of human and *foz/foz* mouse NASH livers [30,38–41] results in cholesterol crystallization [27,31]. Cholesterol crystals activate NLRP3 in LPS-primed macrophages [23,24]. We first demonstrated such activation (measured as IL-1β release) (Fig. 1A) and showed it is substantially inhibited by 10 nM MCC950 (Fig. 1B). Culture supernatant from crystal-exposed BMMs stimulated neutrophil chemotaxis; prior addition of MCC950 blocked this effect (Fig. 1C). Addition of cholesterol crystals to KCs produced similar results, albeit the magnitude of IL-1β release was less (Fig. 1D *vs.* B). We conducted identical experiments on BMMs from *Tlr4*$^{-/-}$ or *Myd88*$^{-/-}$ mice. Lack of TLR4 reduced IL-1β release, while MYD88 was essential for LPS priming of macrophages to release IL-1β in response to cholesterol crystals (Fig. 1A). Addition of crystals to LPS-primed hepatocytes appeared to cause dose-dependent IL-1β release, but the quantum was much less than for KCs and close to the limit of sensitivity for IL-1β detection (Fig. 1E *vs.* D).

MCC950 exhibits good bioavailability after gavage to mice

MCC950 has excellent microsomal stability, does not inhibit major CYP isoforms, has 70% oral bioavailability and a half-life of 3.2 h after oral dosing in mice [26]. For logistic and animal health reasons, we chose to conduct daily administration of drug or vehicle (rather than twice daily). We therefore measured blood levels following gavage of a single dose (20 mg/kg body weight) to *foz/foz* or Wt mice. As shown in Supplementary Fig. 1B, high blood levels of MCC950 were evident at 1 h with no change by 4 h and appreciable trough levels at 24 h.

Treatment with MCC950 blocks hepatic NLRP3 expression and activation in NASH

To test whether MCC950 can block cholesterol crystal-mediated activation of NLRP3 in intact livers with NASH (crystals shown in Supplementary Fig. 2A), we fed *foz/foz* mice atherogenic diet for 16 weeks to cause NASH [29,30,37], then gavaged animals with MCC950 or vehicle for another 8 weeks (experimental design summarized in Supplementary Fig. 1A). Livers of vehicle-treated *foz/foz* mice with NASH exhibited substantial increases in NLRP3 (Fig. 2A), active caspase 1 (but not procaspase 1), pro-IL-1β and IL-1β (Fig. 2B–F). MCC950 reduced expression of all proteins (except pro-IL-1β) to values in vehicle-treated Wt mice (Fig. 2A–F). At 24 weeks, there was a significant increase in circulating IL-1β in vehicle-treated *foz/foz* mice with NASH compared to Wt mice with simple steatosis; MCC950 prevented this increase (Fig. 3A). There were no significant changes in IL-18 between groups (Fig. 3B).

Treatment with MCC950 ameliorates liver injury and inflammation in two murine steatohepatitis models

In atherogenic diet-fed *foz/foz* mice gavaged with vehicle, plasma ALT and AST increased substantially at 16 weeks compared to Wt mice fed the same diet, with further rise by 24 weeks (Fig. 3C and D). Administration of MCC950 abrogated the increase in ALT and AST between 16 and 24 weeks in *foz/foz* mice, and also the moderate further increase in Wt mice (Fig. 3C and D). MCC950 did not cause weight loss in *foz/foz* or Wt mice (Supplementary Fig. 3A). There was also no reduction of hepatomegaly (Supplementary Fig. 3B), or in fasting blood glucose, plasma insulin, adiponectin, cholesterol, or triglyceride (Supplementary Fig. 3C–F). Consistent with this lack of effect on metabolic indices and our earlier observation that insulin drives hepatic cholesterol accumulation [30], there was no difference in cholesterol crystal numbers between livers of MCC950- and vehicle-treated *foz/foz* mice (Supplementary Fig. 2B). In contrast to this lack of effect on the “metabolic drivers” of NASH pathogenesis [6], MCC950 lowered plasma MCP-1 and IL-6 levels (Fig. 3E and F). Likewise, whereas blinded semiquantitative analysis of liver histology showed no effect of MCC950 on steatosis score (Fig. 4A [i]), there was reduction of liver inflammation (Fig. 4B), and a strong trend (not significant) for less ballooning (Fig. 4A [ii]) and lower overall NAS score (Fig. 4A [iii]). The effects of MCC950 on liver inflammation were supported by significant (~50%) suppression of nuclear NF-κB p65 expression (in hepatocytes and inflammatory cells), and in the number of MPO-positive cells (neutrophils) and F4/80-positive cells (macrophages/activated KCs forming crown-like structures [CLS]) (Fig. 4C–E). Importantly, global assessment of liver pathology as “definite NASH”, which was 64% in vehicle-treated *foz/foz* mice, appeared to be less (18%) in MCC950-treated animals, although likely because of the relatively small numbers this apparent difference was not significant (Table 1).

The MCD model shows severe steatohepatitis but is not caused by overnutrition or associated with insulin resistance [28,32,42,43]. Levels of active caspase 1 and IL-1β, and *Asc, Casp1* and *Il1b* mRNA expression were all higher in livers of MCD-fed *vs*. MCS-fed mice. Gavaging MCC950 for 6 weeks significantly lowered their expression (Fig. 5A). As reported [28,32,42,43], MCD diet-fed mice lost weight compared with controls, but MCC950 exerted no separate effect on body weight (data not shown). Livers of MCD-fed

mice showed steatosis with severe lobular inflammation (Fig. 5B), though at the dose used for these experiments (effectively half that used for *foz/foz* mice – see materials and methods) there was no effect of MCC950 on plasma ALT. Hepatic infiltration with neutrophils (MPO) and total macrophages (F4/80) indicated by immunohistochemistry (Fig. 5B), and relevant mRNA transcripts for F4/80, MPO and infiltrating macrophages (*Ly6c* mRNA) increased in MCD *vs.* MCS mouse liver (Supplementary Fig. 4); MCC950 partially (significantly) corrected overexpression of these inflammatory markers (Fig. 5B; Supplementary Fig. 4).

MCC950 retards development of liver fibrosis in MCD diet-induced steatohepatitis and in foz/foz mice with NASH

As expected, MCD diet-fed mice showed increased collagen deposition by Sirius Red staining (Fig. 5C), with corresponding increases in *Col1a1*, connective tissue growth factor (*Ctgf*) and tissue inhibitor of matrix metalloproteinase 1 (*Timp1*) transcripts compared to MCS controls (Fig. 5D). Treatment with MCC950 for 6 weeks appeared to decrease hepatic fibrosis by Sirius Red densitometry (Fig. 5C), and significantly reduced hepatic expression of the aforementioned pro-fibrotic markers (Fig. 5D). In case the dose regimen selected for these experiments was suboptimal (compared with that used for *foz/foz* mouse experiments), we repeated this experiment using the same dose (20 mg/kg body weight) as in *foz/foz* mice administered by gavage once a day for 2 weeks, starting 4 weeks after mice had been fed an MCD diet. There appeared to be substantial Sirius Red-positive material in liver sections of vehicle-treated controls and very little in MCC950-treated mice, although the apparent difference in collagen density fell short of significance ($p = 0.056$) (Supplementary Fig. 5B).

An ideal anti-inflammatory approach to NASH treatment would not only prevent fibrosis development it would also arrest or reverse established liver fibrosis. To test this, we administered MCC950 to *foz/foz* mice already fed atherogenic diet 16 weeks (Supplementary Fig. 1A), at which time fibrotic NASH is established, as confirmed by substantial collagen deposition (Sirius Red densitometry) in vehicle-treated mice (Fig. 6A and B). Following treatment for 8 weeks with the NLRP3 inhibitor, there was ~33% reduction in macroscopic liver fibrosis compared to vehicle-treated controls (Fig. 6A and B), accompanied by significant (but incomplete) suppression of collagen 1 expression, reduced HSC activation (as alpha-smooth muscle actin [α-SMA] expression) and hepatic CTGF (Fig. 6C–F).

Discussion

The most important finding in these studies is that pharmacological inhibition of NLRP3 *in vivo* reduces liver inflammation and hepatocyte injury in metabolic syndrome-related NAFLD with significant reduction in resultant liver fibrosis. Hepatic NLRP3 expression increases during development of experimental and clinical NAFLD [11,13,14,18–20,25], and mice deficient in NLRP3 ($Nlrp3^{-/-}$) or its essential components ($Asc^{-/-}$ and $Casp1^{-/-}$ mice) are protected against fatty liver disease caused by high fat or nutrient-deficient diets [12,14,20]. The present experiments employed atherogenic diet-fed *foz/foz* mice, a NASH model in which animals develop severe obesity, metabolic syndrome and diabetes. In this

clinically relevant model, we showed induction of NLRP3 and evidence of its activation in liver (active caspase 1, IL-1β) in mice with NASH; MCC950 blocked such activation of the NLRP3 inflammasome in liver tissue, with resultant suppression of macrophage (with CLS formation) and neutrophil recruitment. Pharmacological NLRP3 blockade also reduced hepatic expression of pro-IL-1β and normalized hepatic and circulating IL-1β, IL-6 and MCP-1 levels; pro-IL-1β and MCP-1 synthesis is regulated by NF-κB, whose nuclear expression was also suppressed substantially in these experiments [9,18,22,44]. Hepatic NLRP3 expression was also suppressed by MCC950 treatment, most likely because decreased production of IL-1β was, at least in part, responsible for the observed dampening of NF-κB activation. In the MCD model, NLRP3 inflammasome inhibition similarly reduced macrophage and neutrophil infiltration into the liver. Together, these data provide compelling evidence to support earlier work in gene-deleted and dietary models for a central pro-inflammatory role of NLRP3 activation in pathogenesis of NASH.

Our *in vitro* studies combined with the observed effects of MCC950 *in vivo* may provide some insight into why NLRP3 is activated in NASH livers. A dual signal is required to promote NLRP3 macromolecular assembly and caspase 1 activation [16,18,21,22]. It seems possible that gut-derived PAMPs, such as LPS used in our *in vitro* experiments, play such a role in NASH [45,46]. Additional signal-1 molecules include TNF-α and IL-1β. Signal-2 molecules relevant to NASH include crystals and ATP. We showed earlier, and confirmed here (Supplementary Fig. 2A), that cholesterol crystals form in hepatocytes in *foz/foz* mice as well as human NASH [27,31]. These crystals could play their most critical role when hepatocytes undergo necrotic cell death as part of lipotoxicity [34], releasing crystals into the surrounding tissue [47] where they are taken up by KCs and infiltrating macrophages, thus activating NLRP3 with release of large quanta of IL-1β. Here we used cholesterol crystals to activate NLRP3 in macrophages and KCs *in vitro*, simulating the likely uptake of such crystals in the intact liver. We showed that MYD88 is an obligatory signalling intermediate for this pathway, and that it is augmented by TLR4 signaling. A role for TLR4 in experimental NASH receives strong support from other studies. For example, we and Li *et al*. have shown it is part of a high mobility group box 1 (HMGB1) dependent feed-forward pathway of lipotoxic injury to hepatocytes in the early stages of NASH [34,48]. The mechanisms for interaction between TLR4 and NLRP3 include NF-κB-dependent induction of NLRP3 and pro-IL-1β. In turn, IL-1β binding its cognate receptor activates NF-κB [16,22,44], leading to a vicious cycle of pro-inflammatory signalling. It remains possible that HMGB1 and other DAMPs activate both pathways simultaneously, but this requires further studies.

Our results do not support the contention that NLRP3 influences metabolic disorder relevant to NASH pathogenesis [45,46]. Specifically, MCC950 did not alter body weight or the very high plasma insulin, fasting blood glucose, plasma cholesterol and low plasma adiponectin levels in obese *foz/foz* mice, all of which contribute mechanistically to NASH [1,2,5–7]. The different conclusions reached by earlier workers may be due to the breeding of mice with a constitutive NLRP3 deletion leading to microbial dysbiosis [45,46], which is not seen when NLRP3 is inhibited in adult mice. Our data also fail to support a proposed role of IL-1β in contributing to hepatocyte fat deposition in NASH [17,49]. Instead, the beneficial effects of MCC950 inhibition against steatohepatitis were limited to abrogation of the pro-

inflammatory effects of hepatic NLRP3 activation, not to any effect on steatosis or cholesterol crystal deposition which remained unaltered.

The operation of NLRP3 as a pathogenic mechanism in the MCD model indicates that cholesterol crystals are not the only pathway to inflammasome activation in steatohepatitis. Release of ATP from necrotic cells, HMGB1, histones, amyloid and uric acid crystals can each activate NLRP3 via separate but potentially overlapping pathways [15,18,21,22,44], while reactive oxygen species (ROS) and potassium ion fluxes are linked to the effector stages of NLRP3 activation [22]. We and others [42,44] have demonstrated that the predominant lipidomic abnormality in the MCD-fed mice is accumulation of saturated free fatty acids, differing from *foz/foz* mice and human NASH in which free cholesterol is the toxic lipid that distinguishes NASH from simple steatosis [30,38–41]. Saturated free fatty acids and free cholesterol both cause lipotoxicity via JNK1 activation [34,50], leading to mitochondrial injury with generation of ROS. Sources of oxidative stress have been characterized in the MCD model and in human NASH, such as induction of CYPs 2E1 and 4A [32,33]. Whether ROS are sufficient to act alone as second signal (with LPS, TNF-α or IL-1β as signal-1) or augment other inflammasome activators, such as ATP and cholesterol crystals, requires further study.

Liver fibrosis predicts adverse liver outcomes in NAFLD [1–4], so an emphasis of these studies, was to establish whether NLRP3 inhibition reduces liver fibrosis in steatohepatitis. We tested this in two entirely different models [28], because several pathways may interact to promote hepatic fibrogenesis in steatohepatitis. NLRP3 inhibition may combat liver fibrosis because dampening liver inflammation lowers expression of pro-fibrotic cytokines and growth factors (TNF-α, TGF-β, CTGF), and IL-1β may be directly pro-fibrogenic [12,19,44]. Indeed, administration of anakinra, an IL-1β receptor antagonist, improved liver fibrosis in experimental alcoholic hepatitis [17]. Our present results in MCD-fed mice demonstrate that MCC950, an orally available small molecule, affords substantial (though incomplete) protection against hepatic fibrosis when administered at the same time as the disease-inducing diet over 6 weeks, and even when administered for 2 weeks, such a regimen appears to show a moderate (albeit not significant) reduction of collagen deposition. In the more protracted obese/diabetic *foz/foz* model, the 8-week data from 16 to 24 weeks complement this finding, and indicate the potential for NLRP3 inhibitor treatment to arrest or resolve of liver fibrosis once NASH is established. Further experiments with introduction of MCC950 therapy at a later time, are required to test the extent to which NLRP3 blockade reverses advanced stage liver fibrosis in NASH.

In summary, we show here that MCC950, a first-in-class potent and specific NLRP3 inhibitor, improves liver injury, substantially reduces hepatic infiltration with macrophages and neutrophils and modulates fibrotic progression of steatohepatitis in two different models. We demonstrated by tissue studies that these effects resulted from substantial reduction of NLRP3 activation in the liver. It remains possible that NLRP3 activation proceeds in concert with other pro-inflammatory pathways, such as lipotoxicity, oxidative stress and TLR4, but a role for NLRP3 and IL-1β on metabolic regulation and hepatic lipid deposition is not supported by the present findings. While the effect of MCC950 on NASH fibrosis in these models is encouraging, the full potential of inflammasome blockade may

exceed what we observed here as MCC950, which is a test compound for proof-of-principal studies, does not have optimal pharmacokinetics for once a day oral dosing. Development of second generation NLRP3 inhibitors optimized for liver bioavailability and human use will allow testing of whether these agents provide pharmacological resolution of NASH, and whether this novel approach will reverse significant liver fibrosis, its most important outcome.

Supplementary Material

Refer to Web version on PubMed Central for supplementary material.

Acknowledgements

David Povero and Maria Eugenia Inzaugarat kindly assisted with conduct of additional studies in the MCD model in San Diego and assisted with preparation of the figures. The authors also gratefully acknowledge the excellent support of Vanessa Barns and Hans Wang for conduct of animal studies in Canberra.

Financial support

Supported by NIH Project grants R2 AA023574 and U01 AA022489 (to AEF), Australian NHMRC project grants 1084136 and 1044288 (to GCF), and 1086786 (to MAC and AABR), and Deutsche Forschungsgemeinschaft WR 173/3-1 (to AW). Matthew Cooper is an NHMRC Principle Research Fellow (1059354).

References

[1]. Ahmed A, Wong RJ, Harrison SA. Nonalcoholic fatty liver disease review: Diagnosis, treatment, and outcomes. Clin Gastroenterol Hepatol 2015;13: 2062–2070. [PubMed: 26226097]

[2]. Farrell GC, McCullough AJ, Day CP, editors. Non-alcoholic fatty liver disease: A practical guide. Chichester: Wiley-Blackwell; 2013.

[3]. Angulo P, Kleiner DE, Dam-Larsen S, Adams LA, Bjornsson ES, Charatcharoenwitthaya P, et al. Liver fibrosis, but no other histologic features, is associated with long-term outcomes of patients with nonalcoholic fatty liver disease. Gastroenterology 2015;149: 389–397e310. [PubMed: 25935633]

[4]. Torres DM, Harrison SA. Nonalcoholic fatty liver disease: Fibrosis portends a worse prognosis. Hepatology 2015;61: 1462–1464. [PubMed: 25564771]

[5]. Cusi K Role of obesity and lipotoxicity in the development of nonalcoholic steatohepatitis: Pathophysiology and clinical implications. Gastroenterology 2012;142: 711–725. [PubMed: 22326434]

[6]. Larter CZ, Chitturi S, Heydet D, Farrell GC. A fresh look at NASH pathogenesis. Part 1: The metabolic movers. J Gastroenterol Hepatol 2010;25: 672–690. [PubMed: 20492324]

[7]. Neuschwander-Tetri BA. Hepatic lipotoxicity and the pathogenesis of nonalcoholic steatohepatitis: The central role of nontriglyceride fatty acid metabolites. Hepatology 2010;52: 774–788. [PubMed: 20683968]

[8]. Gao B Innate immunity and steatohepatitis: A critical role of another toll (tlr-9). Gastroenterology 2010;139: 27–30. [PubMed: 20639084]

[9]. Kubes P, Mehal WZ. Sterile inflammation in the liver. Gastroenterology 2012;143: 1158–1172. [PubMed: 22982943]

[10]. Maher JJ, Leon P, Ryan JC. Beyond insulin resistance: Innate immunity in nonalcoholic steatohepatitis. Hepatology 2008;48: 670–678. [PubMed: 18666225]

[11]. Csak T, Pillai A, Ganz M, Lippai D, Petrasek J, Park JK, et al. Both bone marrow-derived and non-bone marrow-derived cells contribute to aim2 and nlrp3 inflammasome activation in a myd88-dependent manner in dietary steatohepatitis. Liver Int 2014;34: 1402–1413. [PubMed: 24650018]

[12]. Dixon LJ, Berk M, Thapaliya S, Papouchado BG, Feldstein AE. Caspase-1-mediated regulation of fibrogenesis in diet-induced steatohepatitis. Lab Invest 2012;92: 713–723. [PubMed: 22411067]

[13]. Dixon LJ, Flask CA, Papouchado BG, Feldstein AE, Nagy LE. Caspase-1 as a central regulator of high fat diet-induced non-alcoholic steatohepatitis. PLoS One 2013;8 e56100. [PubMed: 23409132]

[14]. Ganz M, Csak T, Szabo G. High fat diet feeding results in gender specific steatohepatitis and inflammasome activation. World J Gastroenterol 2014;20: 8525–8534. [PubMed: 25024607]

[15]. Huang H, Chen HW, Evankovich J, Yan W, Rosborough BR, Nace GW, et al. Histones activate the NLRP3 inflammasome in Kupffer cells during sterile inflammatory liver injury. J Immunol 2013;191: 2665–2679. [PubMed: 23904166]

[16]. Masters SL. Specific inflammasomes in complex diseases. Clin Immunol 2013;147: 223–228. [PubMed: 23294928]

[17]. Petrasek J, Bala S, Csak T, Lippai D, Kodys K, Menashy V, et al. Il-1 receptor antagonist ameliorates inflammasome-dependent alcoholic steatohepatitis in mice. J Clin Invest 2012;122: 3476–3489. [PubMed: 22945633]

[18]. Szabo G, Petrasek J. Inflammasome activation and function in liver disease. Nat Rev Gastroenterol Hepatol 2015;12: 387–400. [PubMed: 26055245]

[19]. Wree A, McGeough MD, Pena CA, Schlattjan M, Li H, Inzaugarat ME, et al. NLRP3 inflammasome activation is required for fibrosis development in nafld. J Mol Med (Berl) 2014;92: 1069–1082. [PubMed: 24861026]

[20]. Wree A, Eguchi A, McGeough MD, Pena CA, Johnson CD, Canbay A, et al. NLRP3 inflammasome activation results in hepatocyte pyroptosis, liver inflammation, and fibrosis in mice. Hepatology 2014;59: 898–910. [PubMed: 23813842]

[21]. Hara H, Tsuchiya K, Kawamura I, Fang R, Hernandez-Cuellar E, Shen Y, et al. Phosphorylation of the adaptor ASC acts as a molecular switch that controls the formation of speck-like aggregates and inflammasome activity. Nat Immunol 2013;14: 1247–1255. [PubMed: 24185614]

[22]. Schroder K, Tschopp J. The inflammasomes. Cell 2010;140: 821–832. [PubMed: 20303873]

[23]. Duewell P, Kono H, Rayner KJ, Sirois CM, Vladimer G, Bauernfeind FG, et al. NLRP3 inflammasomes are required for atherogenesis and activated by cholesterol crystals. Nature 2010;464: 1357–1361. [PubMed: 20428172]

[24]. Rajamaki K, Lappalainen J, Oorni K, Valimaki E, Matikainen S, Kovanen PT, et al. Cholesterol crystals activate the NLRP3 inflammasome in human macrophages: A novel link between cholesterol metabolism and inflammation. PLoS One 2010;5 e11765. [PubMed: 20668705]

[25]. Csak T, Ganz M, Pespisa J, Kodys K, Dolganiuc A, Szabo G. Fatty acid and endotoxin activate inflammasomes in mouse hepatocytes that release danger signals to stimulate immune cells. Hepatology 2011;54: 133–144. [PubMed: 21488066]

[26]. Coll RC, Robertson AA, Chae JJ, Higgins SC, Munoz-Planillo R, Inserra MC, et al. A small-molecule inhibitor of the nlrp3 inflammasome for the treatment of inflammatory diseases. Nat Med 2015;21: 248–255. [PubMed: 25686105]

[27]. Ioannou GN, Haigh WG, Thorning D, Savard C. Hepatic cholesterol crystals and crown-like structures distinguish NASH from simple steatosis. J Lipid Res 2013;54: 1326–1334. [PubMed: 23417738]

[28]. Larter CZ, Yeh MM. Animal models of NASH: Getting both pathology and metabolic context right. J Gastroenterol Hepatol 2008;23: 1635–1648. [PubMed: 18752564]

[29]. Larter CZ, Yeh MM, Van Rooyen DM, Teoh NC, Brooling J, Hou JY, et al. Roles of adipose restriction and metabolic factors in progression of steatosis to steatohepatitis in obese, diabetic mice. J Gastroenterol Hepatol 2009;24: 1658–1668. [PubMed: 19788606]

[30]. Van Rooyen DM, Larter CZ, Haigh WG, Yeh MM, Ioannou G, Kuver R, et al. Hepatic free cholesterol accumulates in obese, diabetic mice and causes nonalcoholic steatohepatitis. Gastroenterology 2011;141: 1393–1403. [PubMed: 21703998]

[31]. Ioannou GN, Van Rooyen DM, Savard C, Haigh WG, Yeh MM, Teoh NC, et al. Cholesterol-lowering drugs cause dissolution of cholesterol crystals and disperse Kupffer cell crown-like structures during resolution of nash. J Lipid Res 2015;56: 277–285. [PubMed: 25520429]

[32]. Leclercq IA, Farrell GC, Field J, Bell DR, Gonzalez FJ, Robertson GR. Cyp2e1 and Cyp4a as microsomal catalysts of lipid peroxides in murine nonalcoholic steatohepatitis. J Clin Invest 2000;105: 1067–1075. [PubMed: 10772651]

[33]. Robertson G, Leclercq I, Farrell GC. Nonalcoholic steatosis and steatohepatitis. II. Cytochrome P-450 enzymes and oxidative stress. Am J Physiol Gastrointest Liver Physiol 2001;281: G1135–G1139. [PubMed: 11668021]

[34]. Gan LT, Van Rooyen DM, Koina ME, McCuskey RS, Teoh NC, Farrell GC. Hepatocyte free cholesterol lipotoxicity results from JNK1-mediated mitochondrial injury and is HMGB1 and TLR4-dependent. J Hepatol 2014;61: 1376–1384. [PubMed: 25064435]

[35]. Froh M, Konno A, Thurman RG. Isolation of liver Kupffer cells. Curr Protoc Toxicol 2003; Chapter 14: Unit14.14.

[36]. Teoh NC, Ajamieh H, Wong HJ, Croft K, Mori T, Allison AC, et al. Microparticles mediate hepatic ischemia-reperfusion injury and are the targets of diannexin (ASP8597). PLoS One 2014;9 e104376. [PubMed: 25222287]

[37]. Farrell GC, Mridha AR, Yeh MM, Arsov T, Van Rooyen DM, Brooling J, et al. Strain dependence of diet-induced NASH and liver fibrosis in obese mice is linked to diabetes and inflammatory phenotype. Liver Int 2014;34: 1084–1093. [PubMed: 24107103]

[38]. Caballero F, Fernandez A, De Lacy AM, Fernandez-Checa JC, Caballeria J, Garcia-Ruiz C. Enhanced free cholesterol, SREBP-2 and STAR expression in human NASH. J Hepatol 2009;50: 789–796. [PubMed: 19231010]

[39]. Min HK, Kapoor A, Fuchs M, Mirshahi F, Zhou H, Maher J, et al. Increased hepatic synthesis and dysregulation of cholesterol metabolism is associated with the severity of nonalcoholic fatty liver disease. Cell Metab 2012;15: 665–674. [PubMed: 22560219]

[40]. Musso G, Gambino R, Cassader M. Cholesterol metabolism and the pathogenesis of non-alcoholic steatohepatitis. Prog Lipid Res 2013;52: 175–191. [PubMed: 23206728]

[41]. Puri P, Baillie RA, Wiest MM, Mirshahi F, Choudhury J, Cheung O, et al. A lipidomic analysis of nonalcoholic fatty liver disease. Hepatology 2007;46: 1081–1090. [PubMed: 17654743]

[42]. Larter CZ, Yeh MM, Haigh WG, Williams J, Brown S, Bell-Anderson KS, et al. Hepatic free fatty acids accumulate in experimental steatohepatitis: Role of adaptive pathways. J Hepatol 2008;48: 638–647. [PubMed: 18280001]

[43]. Pickens MK, Yan JS, Ng RK, Ogata H, Grenert JP, Beysen C, et al. Dietary sucrose is essential to the development of liver injury in the methioninecholine-deficient model of steatohepatitis. J Lipid Res 2009;50: 2072–2082. [PubMed: 19295183]

[44]. Ouyang X, Ghani A, Mehal WZ. Inflammasome biology in fibrogenesis. Biochim Biophys Acta 2013;1832: 979–988. [PubMed: 23562491]

[45]. Henao-Mejia J, Elinav E, Jin C, Hao L, Mehal WZ, Strowig T, et al. Inflammasome-mediated dysbiosis regulates progression of NAFLD and obesity. Nature 2012;482: 179–185. [PubMed: 22297845]

[46]. Wen H, Ting JP, O'Neill LA. A role for the NLRP3 inflammasome in metabolic diseases–did warburg miss inflammation? Nat Immunol 2012;13: 352–357. [PubMed: 22430788]

[47]. Ioannou GN. The role of cholesterol in the pathogenesis of NASH. Trends Endocrinol Metab 2016;27: 84–95. [PubMed: 26703097]

[48]. Li L, Chen L, Hu L, Liu Y, Sun HY, Tang J, et al. Nuclear factor high-mobility group box1 mediating the activation of Toll-like receptor 4 signaling in hepatocytes in the early stage of nonalcoholic fatty liver disease in mice. Hepatology 2011;54: 1620–1630. [PubMed: 21809356]

[49]. Miura K, Kodama Y, Inokuchi S, Schnabl B, Aoyama T, Ohnishi H, et al. Toll-like receptor 9 promotes steatohepatitis by induction of interleukin-1beta in mice. Gastroenterology 2010;139: 323–334e327. [PubMed: 20347818]

[50]. Kakisaka K, Cazanave SC, Fingas CD, Guicciardi ME, Bronk SF, Werneburg NW, et al. Mechanisms of lysophosphatidylcholine-induced hepatocyte lipoapoptosis. Am J Physiol Gastrointest Liver Physiol 2012;302: G77–G84. [PubMed: 21995961]

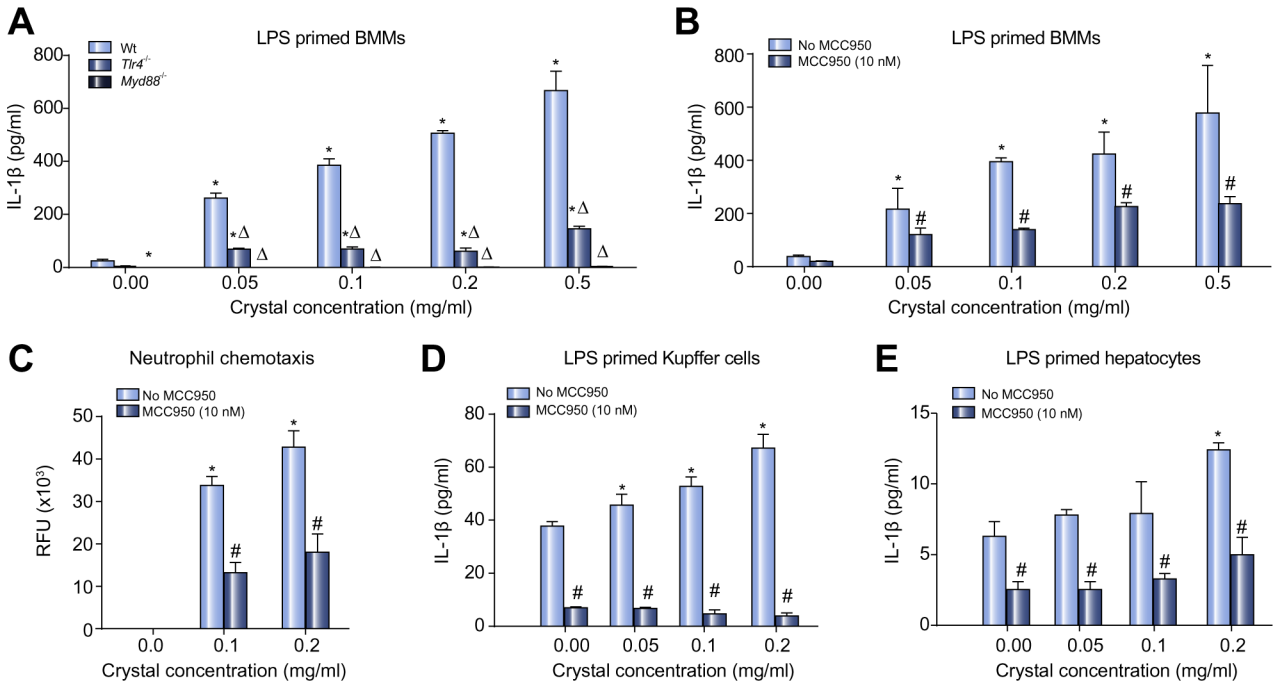

Fig. 1. Cholesterol crystals provoke IL-1β release and neutrophil recruitment by macrophages and Kupffer cells, which is inhibited by MCC950.

(A) Effects of cholesterol crystals on IL-1β release for LPS-primed bone marrow macrophages (BMM) from wild-type (Wt), *Tlr4*$^{-/-}$, and *Myd88*$^{-/-}$ mice. (B) MCC950 (10 nM) inhibits IL-1β production from Wt BMMs. (C) Enriched culture medium from crystal activated BMMs stimulates neutrophil chemotaxis. (D) Cholesterol crystals stimulate IL-1β release from Kupffer cells, but (E) minimally in hepatocytes. *p <0.05 *vs.* no crystals. $^{\Delta}p$ <0.05 *vs.* Wt. $^{\#}p$ <0.05 MCC950 *vs.* untreated, by Mann-Whitney *U* test, n = 9–12.

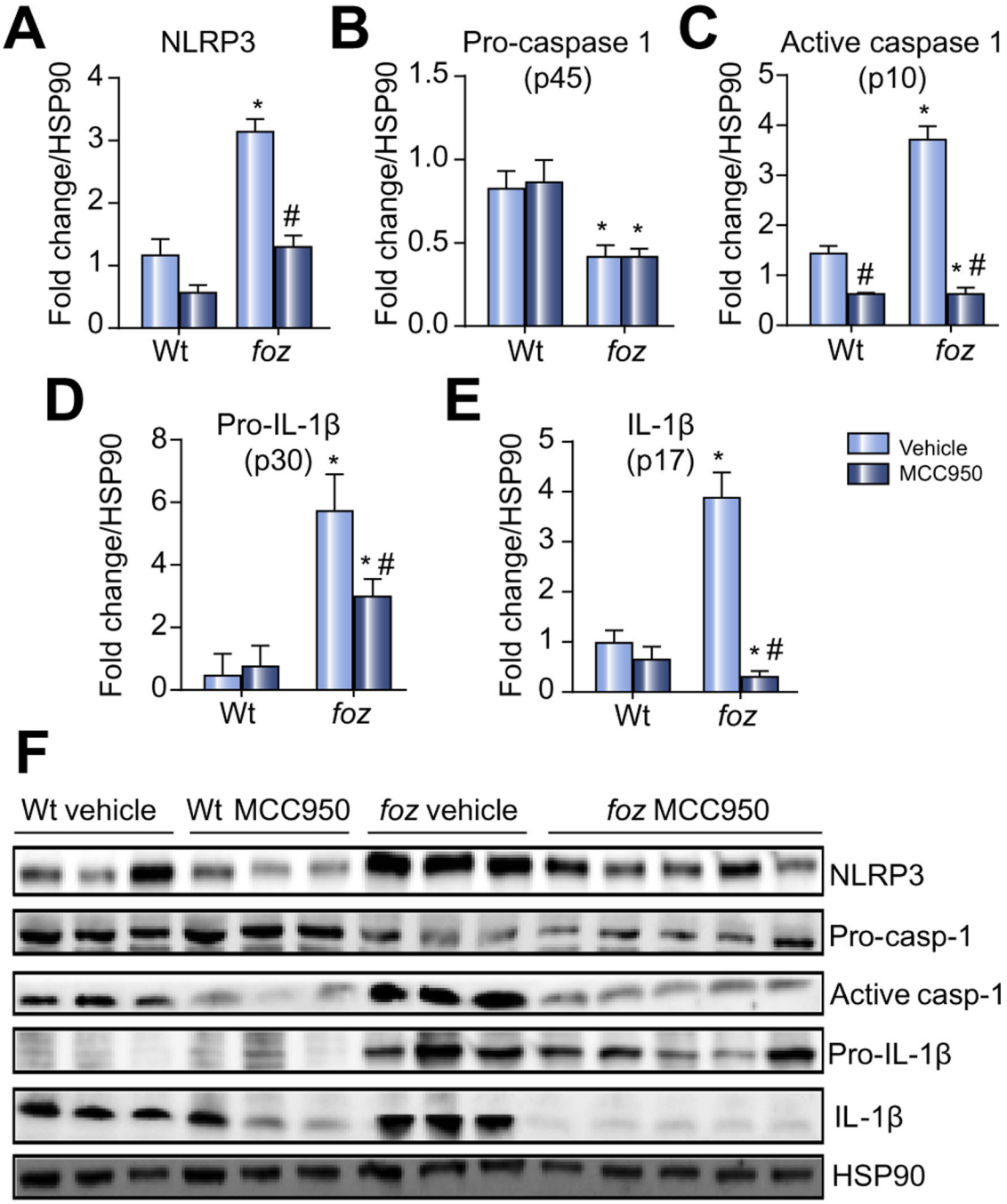

Fig. 2. Effects of conditions causing NASH on hepatic expression of NLRP3, pro-caspase 1, active caspase 1, pro-IL-1β and IL-1β.

(A) NLRP3 in wild-type (Wt) and *foz/foz* mice after 24 weeks atherogenic diet, and gavage during the last 8 weeks with vehicle (saline) or MCC950. (B) Hepatic pro-caspase 1 (p45), (C) active caspase 1 (p10), (D) pro-IL-1β (p30), and (E) IL-1β (p17). (F) Representative Western blot analyses from same experiments, with heat shock protein 90 (HSP90) as loading controls. $^{*}p < 0.05$ *vs.* Wt. $^{\#}p < 0.05$ MCC950 *vs.* vehicle, by one-way ANOVA, n = 6–10 animals/group.

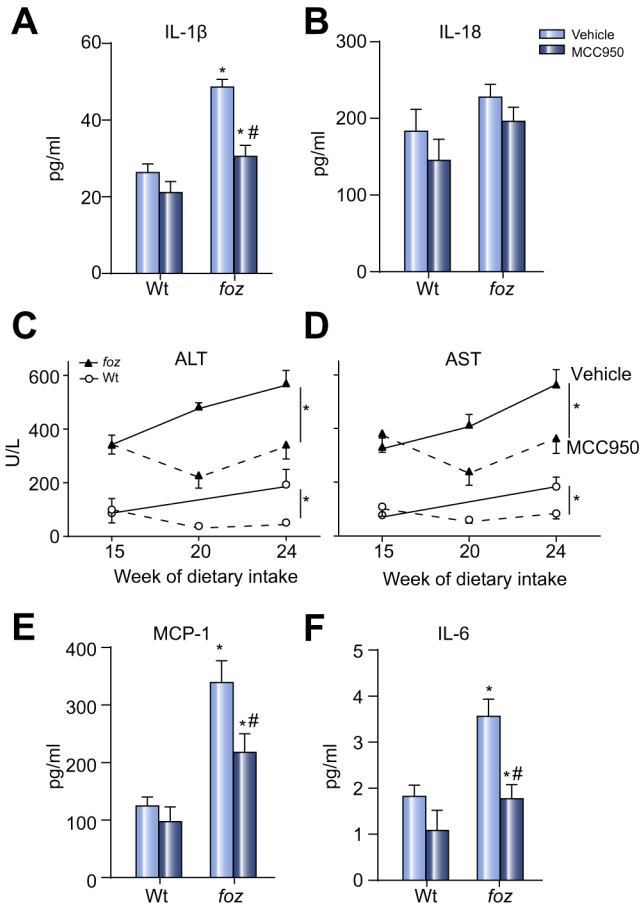

Fig. 3. Effects of MCC950 *vs*. vehicle on circulating cytokines/chemokines and transaminases in mice with NASH.

(A) Plasma IL-1β, (B) plasma IL-18, (C) ALT, (D) AST, (E) macrophage chemotactic protein 1 (MCP-1), (F) IL-6. Same mice as in Fig. 2. $^{*}p$ <0.05 or less *vs*. Wt. $^{\#}p$ <0.05 MCC950 *vs*. vehicle, by one-way ANOVA, n = 11–13 animals/group, same animals as in Fig. 2.

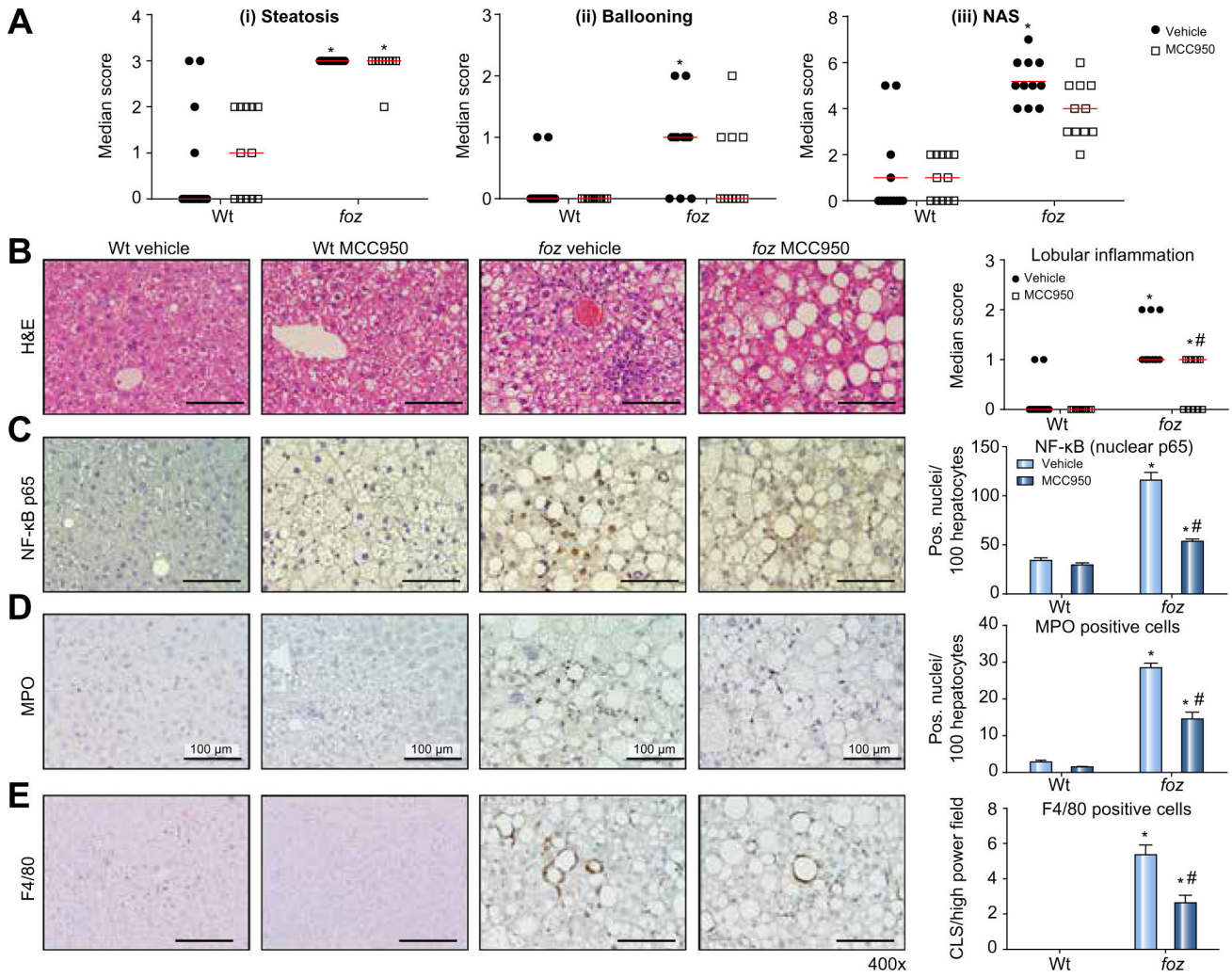

Fig. 4. MCC950 reverses NASH pathology.

(A) (i) Steatosis, (ii) hepatocyte ballooning, and (iii) NAFLD activity score (NAS) in Wt and *foz/foz* mice after 24 weeks atherogenic diet, and gavage during last 8 weeks with vehicle or MCC950. (B) Representative H&E-stained liver sections demonstrating inflammation in atherogenic *foz/foz* mouse liver (vehicle) is abolished by MCC950, with reduction of lobular inflammation score. (C) NF-κB activation (nuclear p65) is suppressed, as are, (D) myeloperoxidase (MPO) positive neutrophils, and (E) F4/80 positive macrophages and Kupffer cells as crown-like structures (CLS). Same experiments as Figs. 2 and 3. $*p < 0.05$ *vs.* Wt. $^{\#}p < 0.05$ MCC950 *vs.* vehicle, by one-way ANOVA, n = 11–13 animals/group. Scale bar: 100 μm.

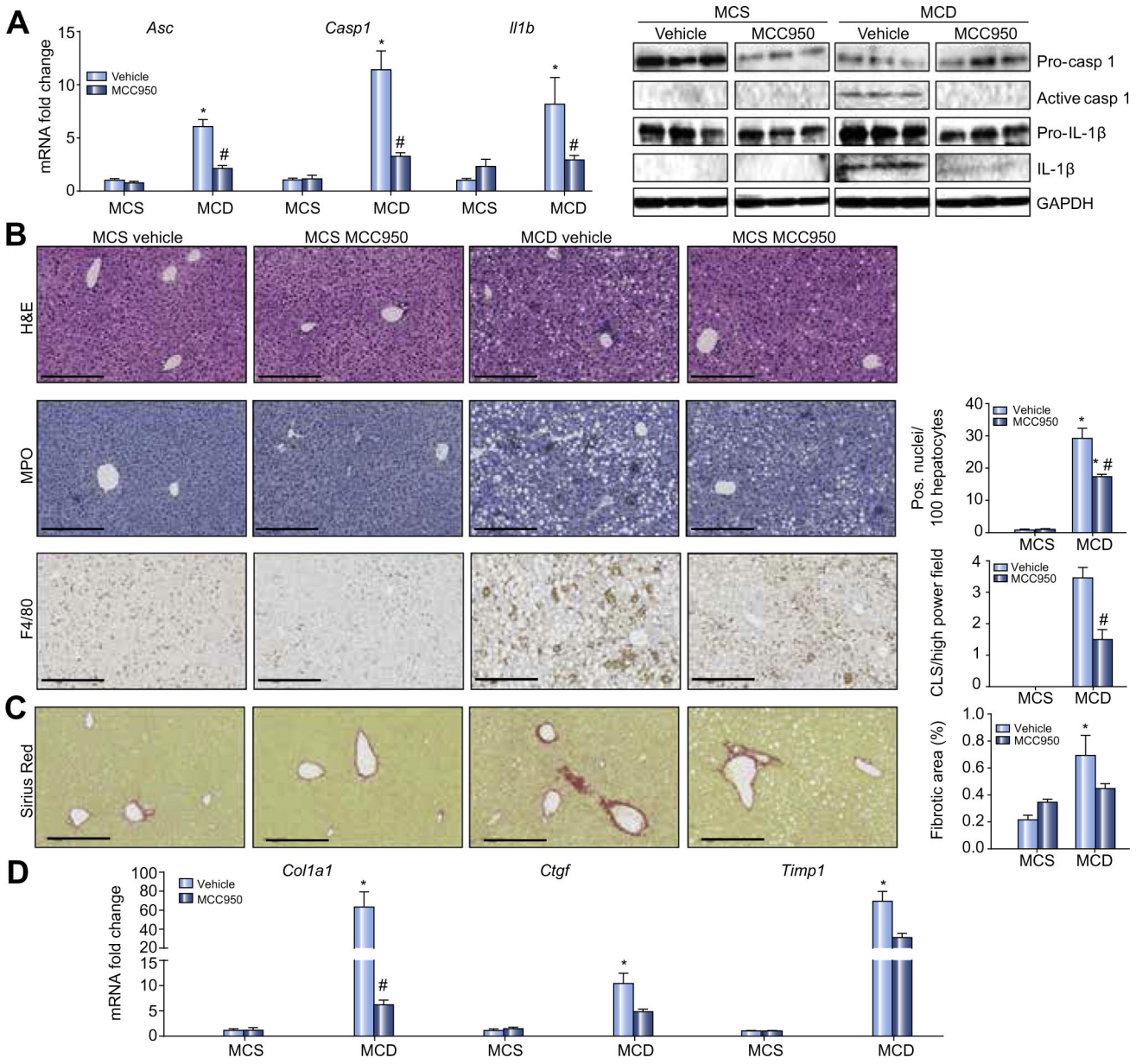

Fig. 5. In MCD-fed mice MCC950 suppresses hepatic NLRP3 inflammasome activation, inflammatory cell infiltration and fibrosis.

(A) Hepatic *Asc, Casp1* and *Il1b* mRNA in mice fed MCD or MCS diets, and gavaged MCC950 or vehicle for 6 weeks. To right, representative Western blot analyses of pro-caspase 1, active caspase 1, pro-IL-1β and IL-1β: GAPDH loading control. (B) Representative H&E-stained liver sections. To right number of infiltrating neutrophils and F4/80-positive cells. (C) Representative Sirius Red-stained liver sections, and percentage fibrotic area. (D) mRNA expression of *Col1a1, Ctgf* and *Timp1*. Data: mean ± SEM, *p <0.05 MCS *vs*. MCD, $^{\#}p$ <0.05 vehicle *vs*. MCC950 by one-way ANOVA, n = 8 animals/ group. Scale bar: 100 μm.

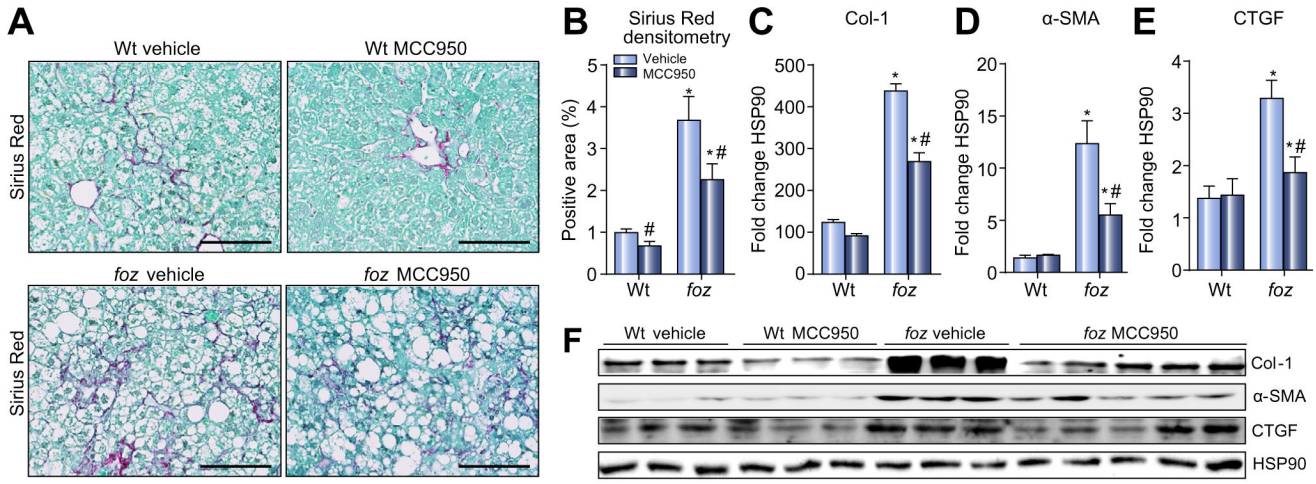

Fig. 6. MCC950 suppresses liver fibrosis in obese, diabetic mice with NASH.

(A) Sirius Red-stained liver sections from Wt and *foz/foz* mice after 24 weeks atherogenic diet intake and gavage during the last 8 weeks with vehicle or MCC950 (same mice as in Figs. 2–4). (B) Collagen area by Sirius Red densitometry. (C) Changes in collagen 1α (Col-1), (D) alpha-smooth muscle actin (α-SMA), (E) connective tissue growth factor (CTGF), and (F) representative Western blot analyses. Heat shock protein 90 (HSP90) as loading control. $*p < 0.05$ or less *vs.* Wt. $^{\#}p < 0.05$ MCC950 *vs.* vehicle, by one-way ANOVA, n = 6–10 animals/group. Scale bar: 100 μm.

Table 1.

Global assessment of NAFLD pathology.

Croups	n	No steatosis	NAFLD, but not NASH	Borderline NASH	Definite NASH
Wt vehicle	13	9 (70%)	2 (15%)	2 (15%)	0
Wt MCC950	12	5 (42%)	7 (58%)	0	0
foz vehicle	11	0	3 (27%)	1 (9.1%)	7 (64%)
foz MCC950	11	0	7 (64%)	2 (18%)	2 (18%)

J Hepatol. Author manuscript; available in PMC 2019 May 27.